Supplement of Geosci. Model Dev., 11, 989–1008, 2018
https://doi.org/10.5194/gmd-11-989-2018-supplement

Geoscientific
Model Development
Open Access

Supplement of

Revised mineral dust emissions in the atmospheric chemistry–climate model EMAC (MESSy 2.52 DU_Astitha1 KKDU2017 patch)

Klaus Klingmüller et al.

Correspondence to: Klaus Klingmüller (k.klingmueller@mpic.de)

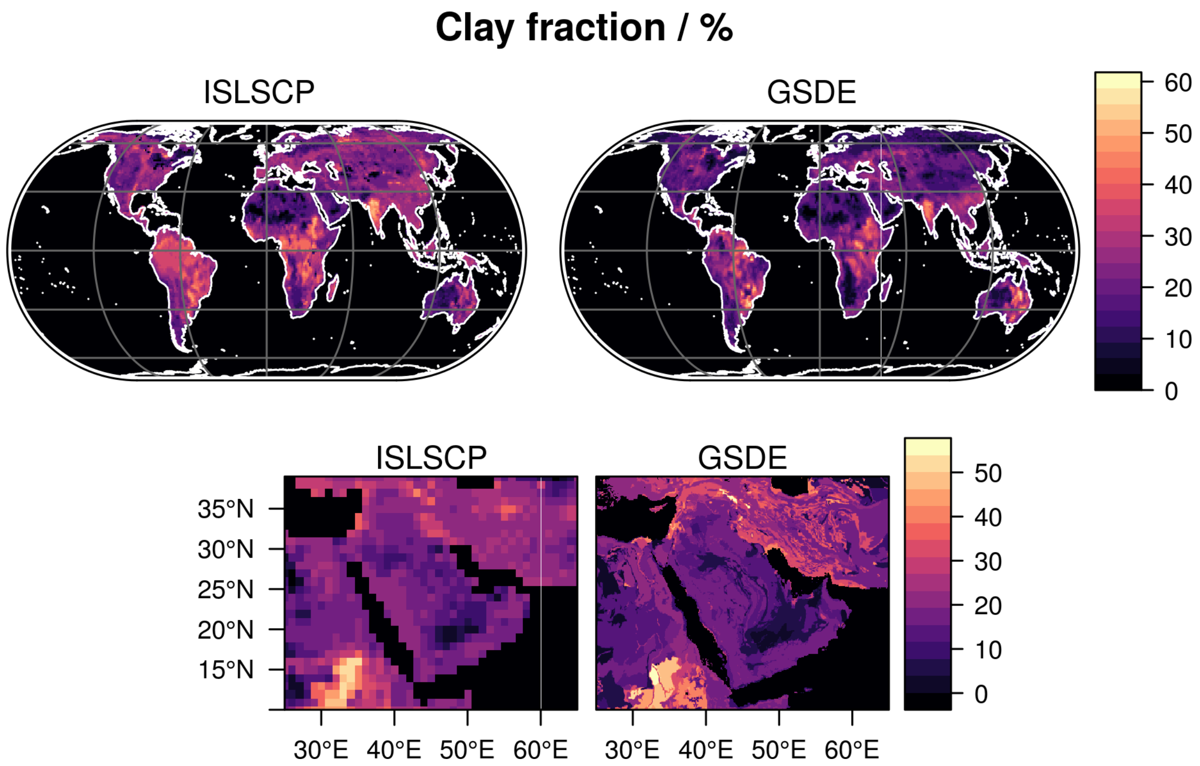

Figure S1: The clay fraction of the topmost soil layer used by Astitha et al. (2012) and in our reference simulation (ISLSCP, Scholes and Brown de Colstoun 2011), and the fraction used by our revised dust emission scheme and in the validation simulation (GSDE, Shangguan et al. 2014). The magnified view of the Middle East (bottom) illustrates the difference in resolution.

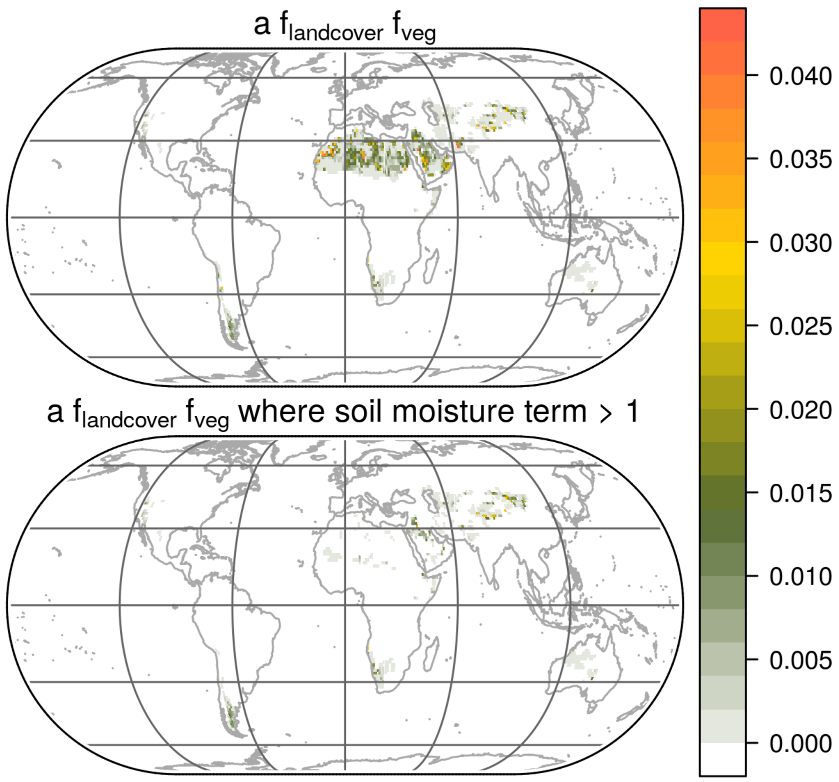

Figure S2: The emission factor $a f_{\text{landcover}} f_{\text{veg}}$ in the reference simulation globally (top) and where the soil moisture term would increase the threshold surface friction velocity (bottom) during the month July. The soil moisture term affects only a minor fraction of the total emissions and predominantly reduces emissions from the Middle East, Central Asia and the Southern Cone; for none of these regions the emissions are overestimated by the two emission schemes omitting the soil moisture term.

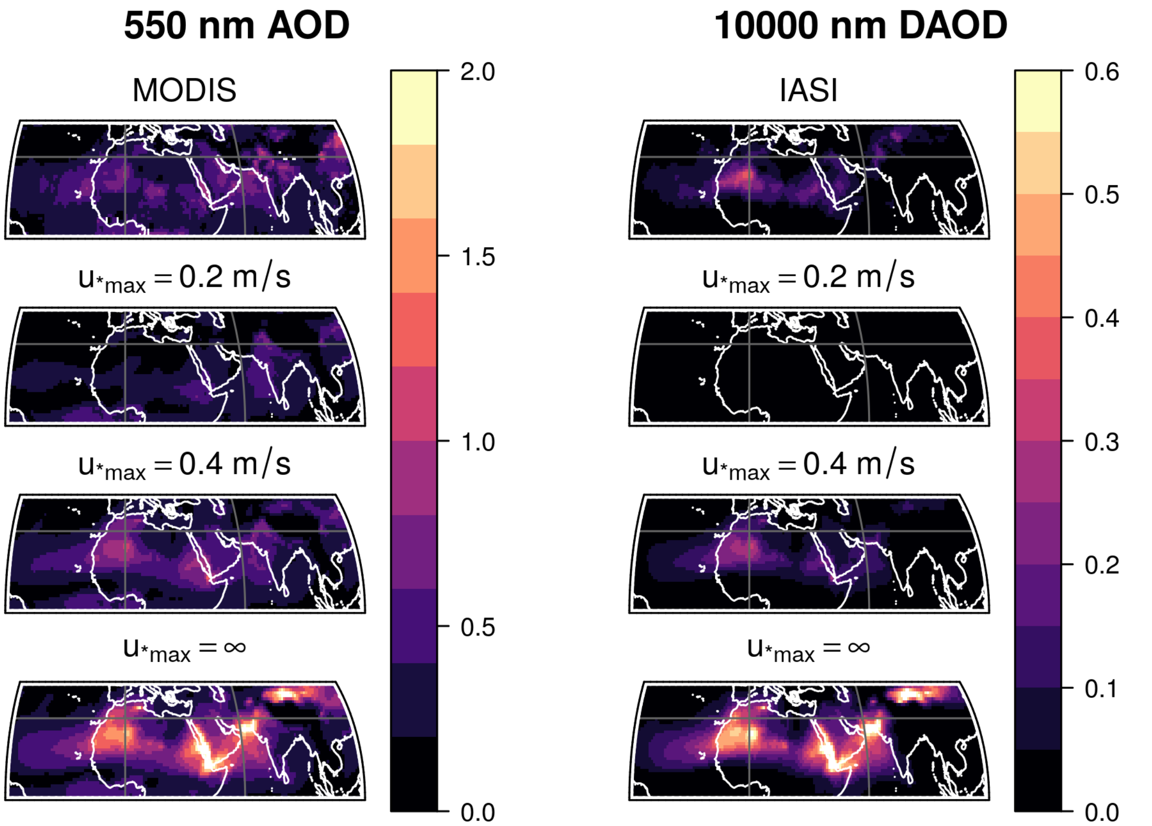

Figure S3: Dependency of 550 nm AOD (left) and 10 μm DAOD (right) for August 2010 on the surface friction velocity limit $u_{*\max}$. Without limit (bottom), dust emissions from regions with steep slopes (e.g., between the Taklamakan Desert and the Himalayas, in Ethiopia/Eritrea and Pakistan) where emissions are not suppressed by landcover classification, vegetation or topography are dominating the emission distribution. A too low limit (0.2 m/s, second row) inhibits emissions too strongly. Values around 0.4 m/s (third row, results from the validation simulation) yield good agreement with MODIS and IASI observations (top).

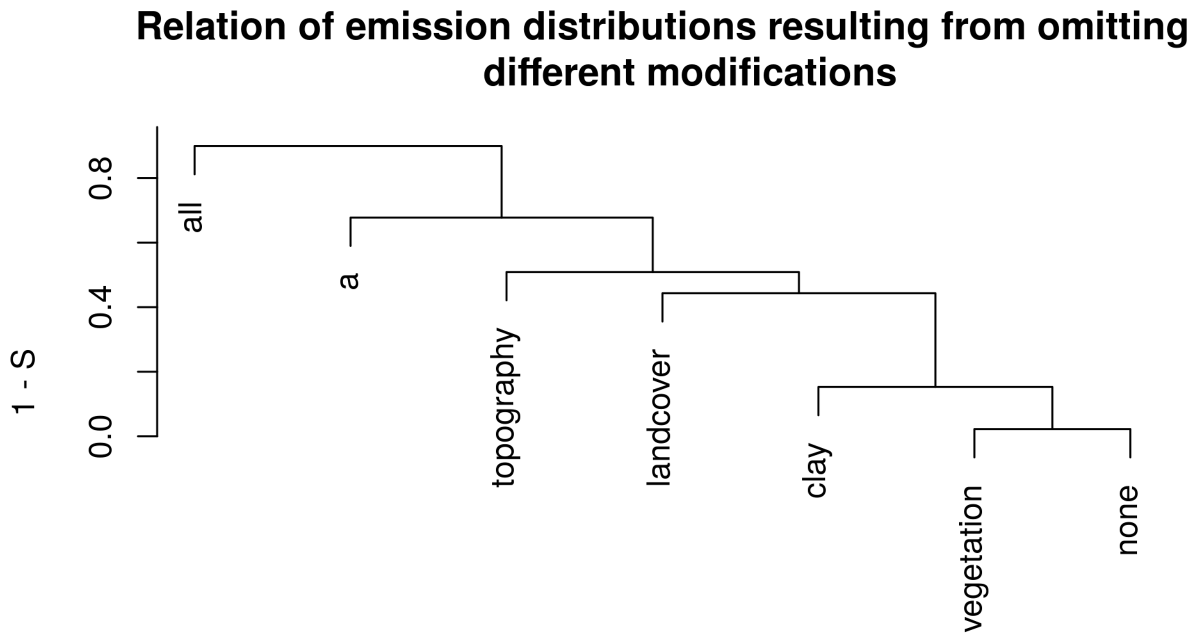

Figure S4: Skill score based complete-linkage cluster dendrogram of the emission factor $a\ f_{\mathrm{landcover}}\ f_{\mathrm{veg}}\ N\ S_{\mathrm{topo}}$ during July 2011 omitting the modifications to either sand blasting efficiency a, topography factor, landcover, clay fraction, vegetation, all combined or none. All data have been regridded to T106 resolution as in the left column of Fig. 7. The modifications to sand blasting efficiency a, topography factor and landcover have a larger impact than the updates of clay fraction and vegetation data.

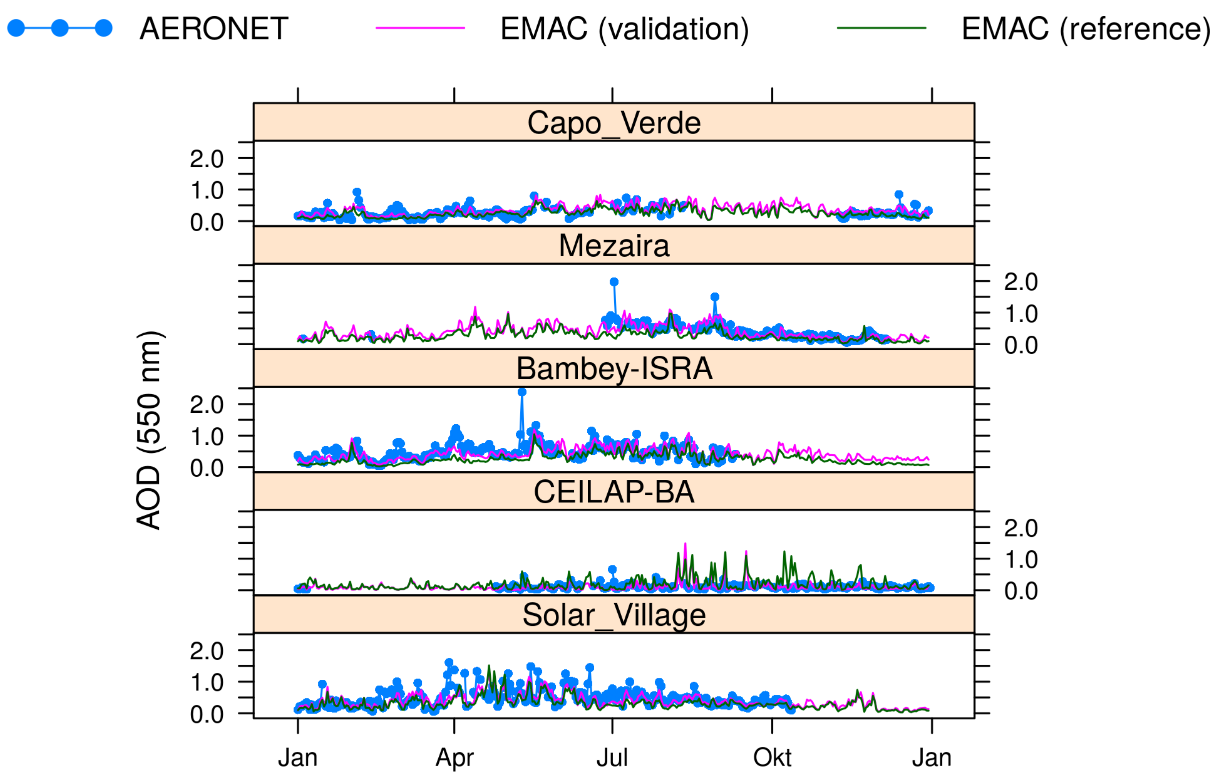

Figure S5: Time series of the daily mean AOD at the AERONET stations with the heighest skill score increase due to the emission scheme revision.

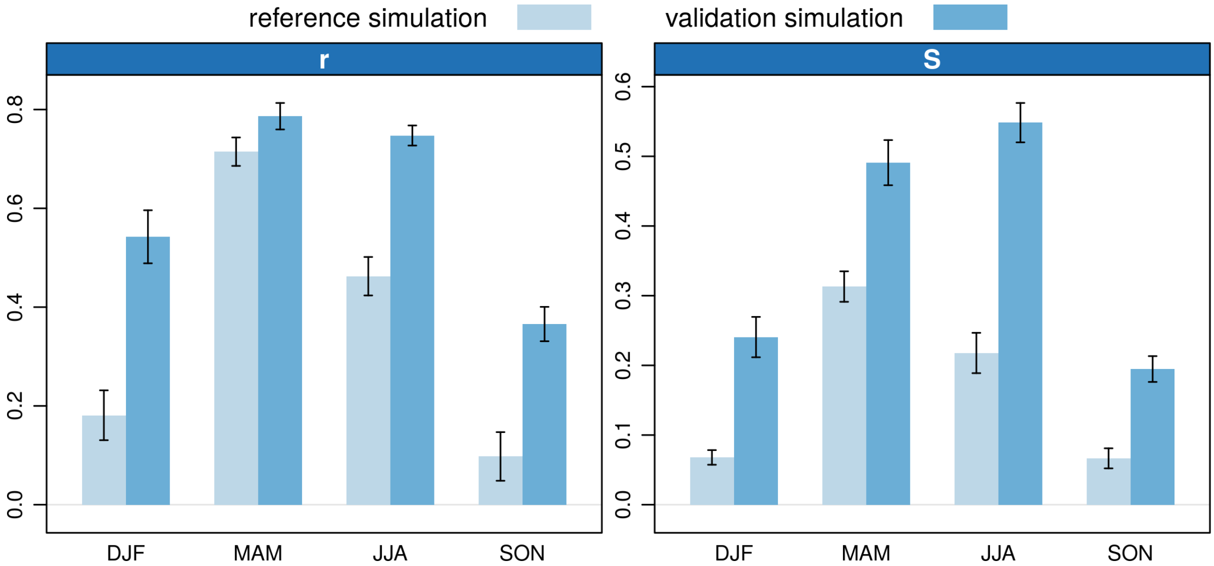

Figure S6: Spatial agreement of the seasonal 550 nm AOD distribution over the Arabian Peninsula (including Syria, Iraq and Jordan) observed by MODIS and obtained by EMAC. The solid bars depict the correlation coefficient (left) and skill score (right), the errorbars indicate the corresponding standard deviation estimated based on jackknife resampling of the pixel values.

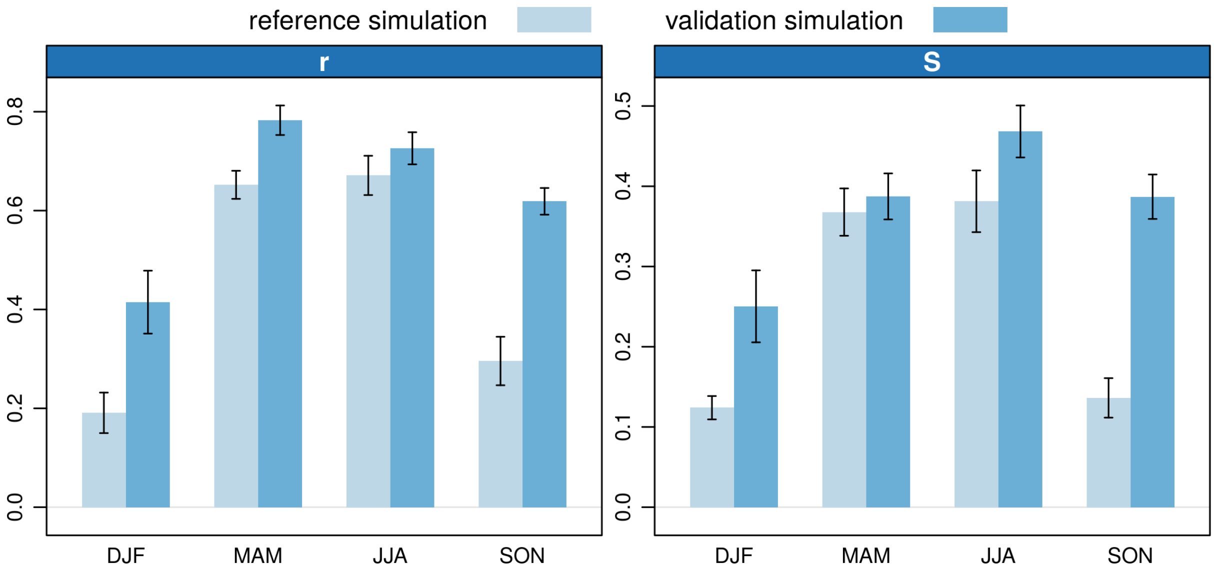

Figure S7: Spatial agreement of the seasonal 10 μm DAOD distribution over the Arabian Peninsula (including Syria, Iraq and Jordan) observed by IASI and obtained by EMAC. The solid bars depict the correlation coefficient (left) and skill score (right), the errorbars indicate the corresponding standard deviation estimated based on jackknife resampling of the pixel values.

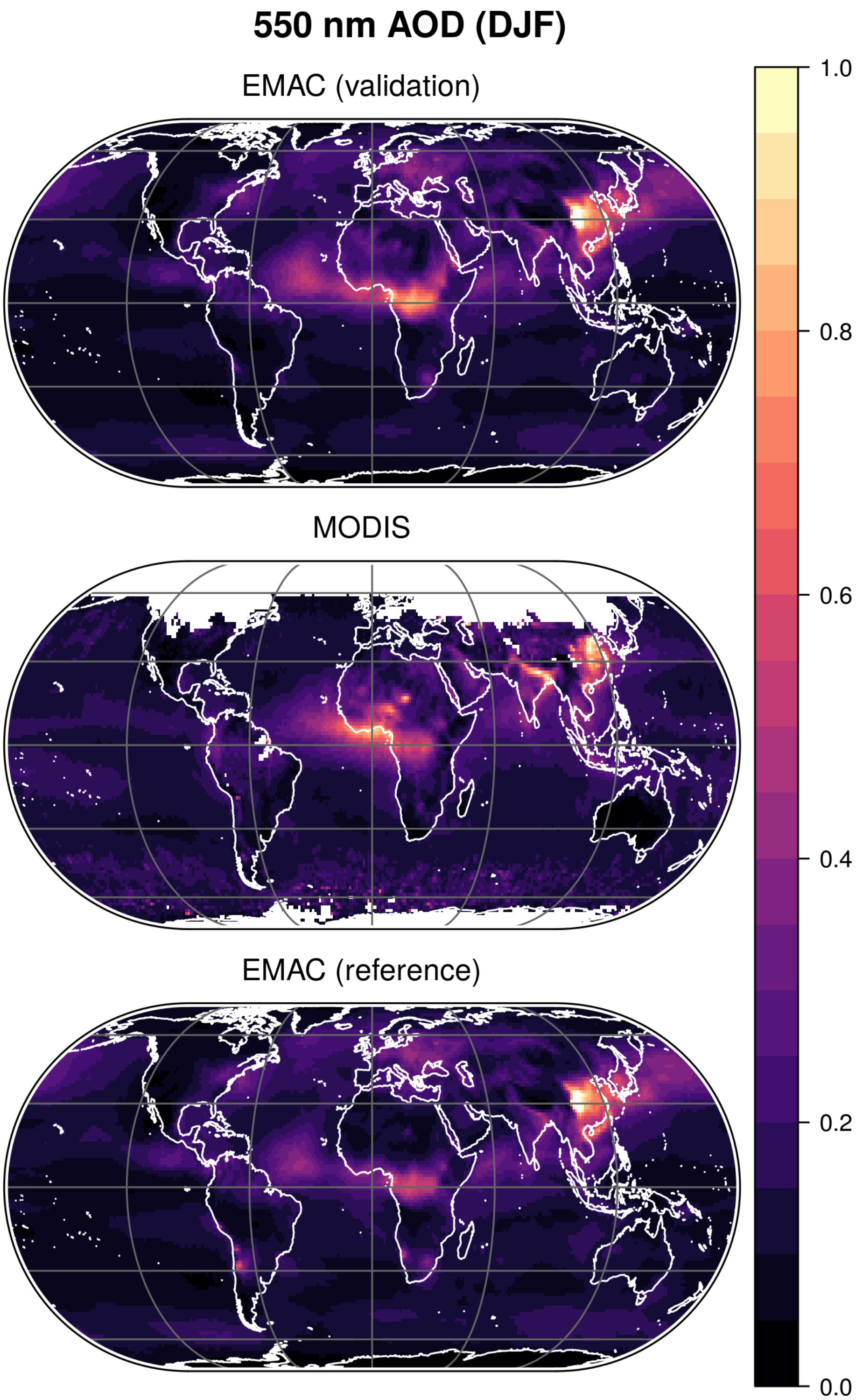

Figure S8: 550 nm AOD during winter (December, January, February) observed by MODIS (centre) and simulated by EMAC with (“validation”, top) and without (“reference”, bottom) revision of the dust emission scheme.

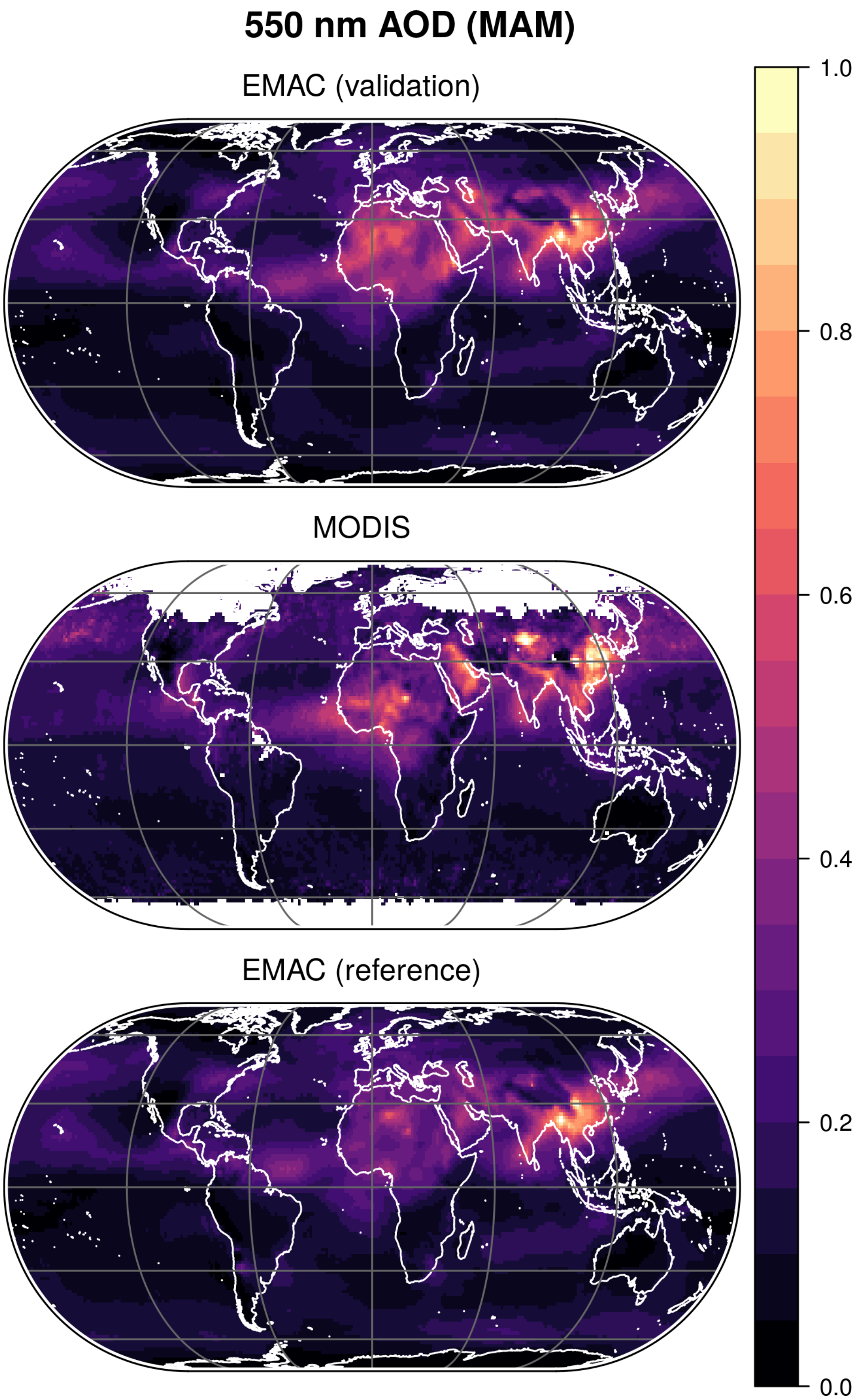

Figure S9: 550 nm AOD during spring (March, April, May) observed by MODIS (centre) and simulated by EMAC with (“validation”, top) and without (“reference”, bottom) revision of the dust emission scheme.

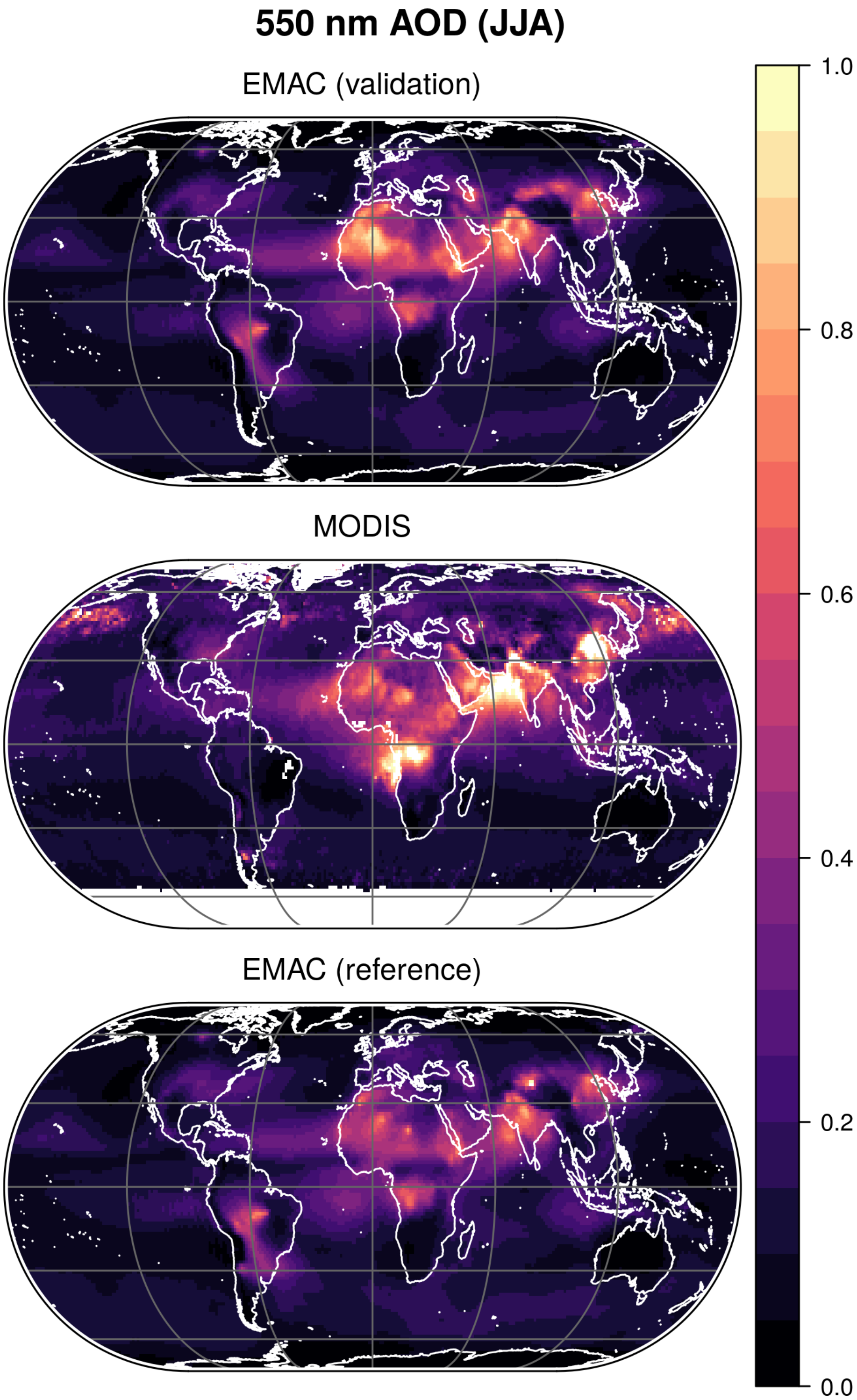

Figure S10: 550 nm AOD during summer (June, July, August) observed by MODIS (centre) and simulated by EMAC with ("validation", top) and without ("reference", bottom) revision of the dust emission scheme.

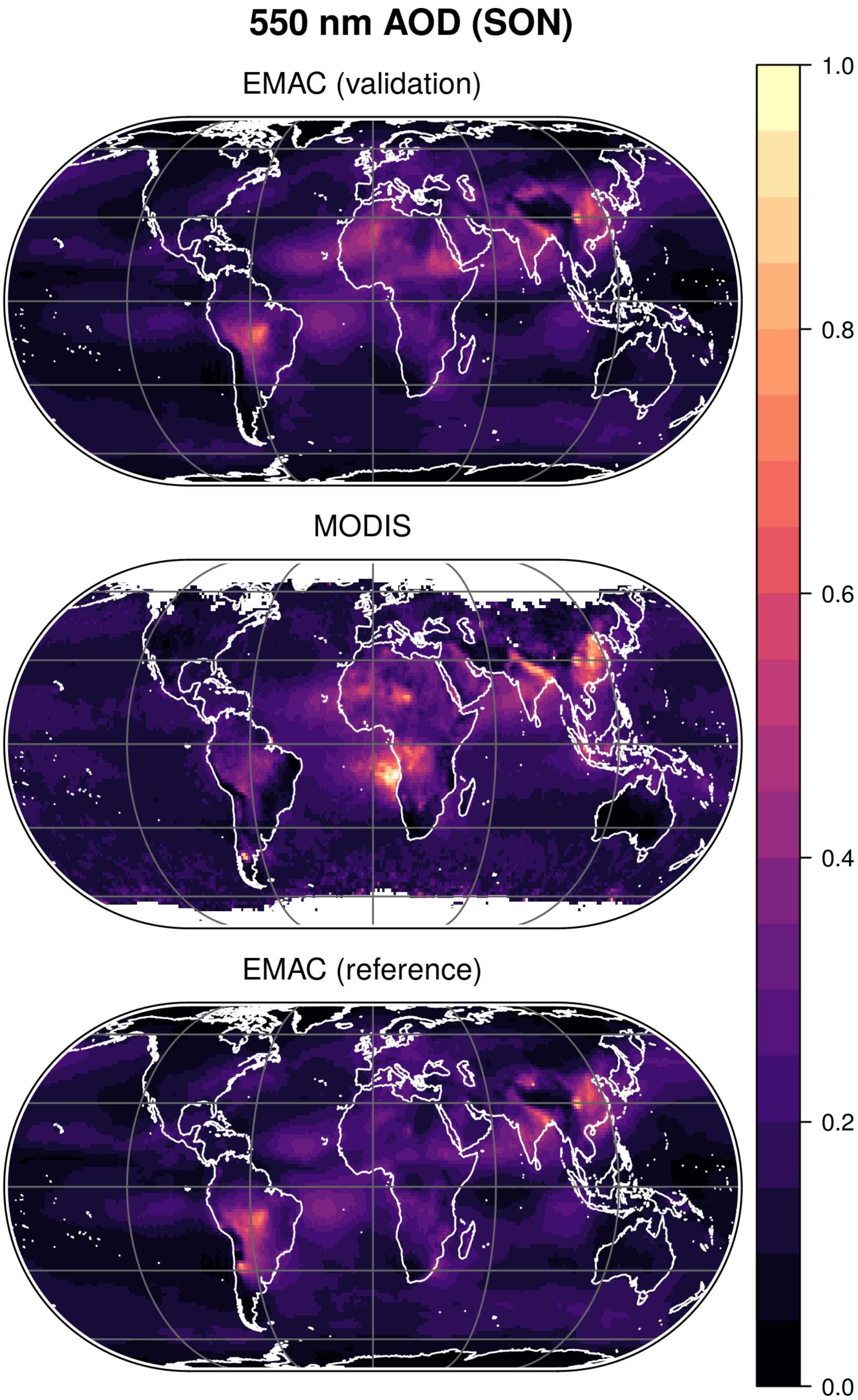

Figure S11: 550 nm AOD during autumn (September, October, November) observed by MODIS (centre) and simulated by EMAC with ("validation", top) and without ("reference", bottom) revision of the dust emission scheme.

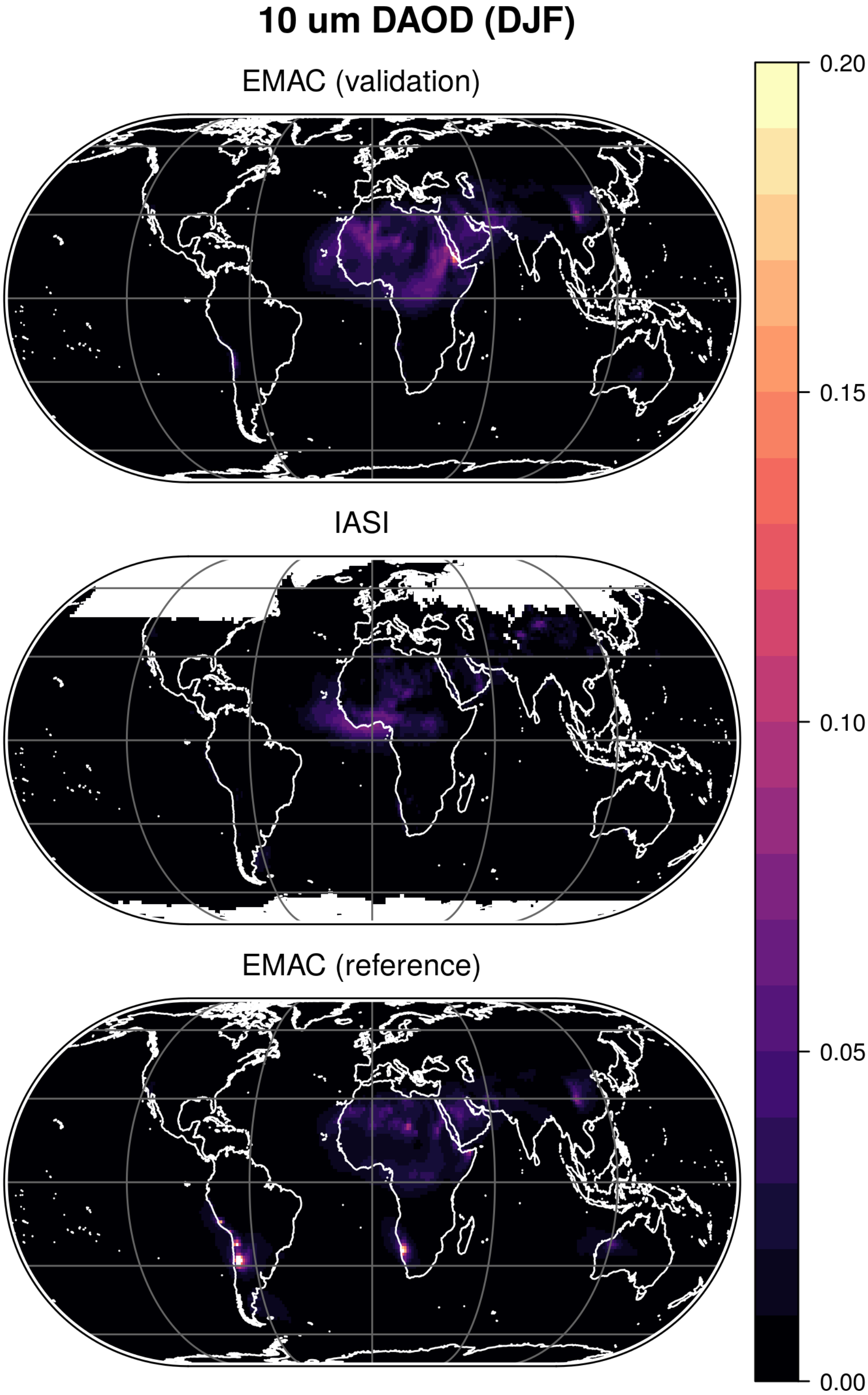

Figure S12: 10000 nm DAOD during winter (December, January, February) observed by IASI (centre) and simulated by EMAC with ("validation", top) and without ("reference", bottom) revision of the dust emission scheme.

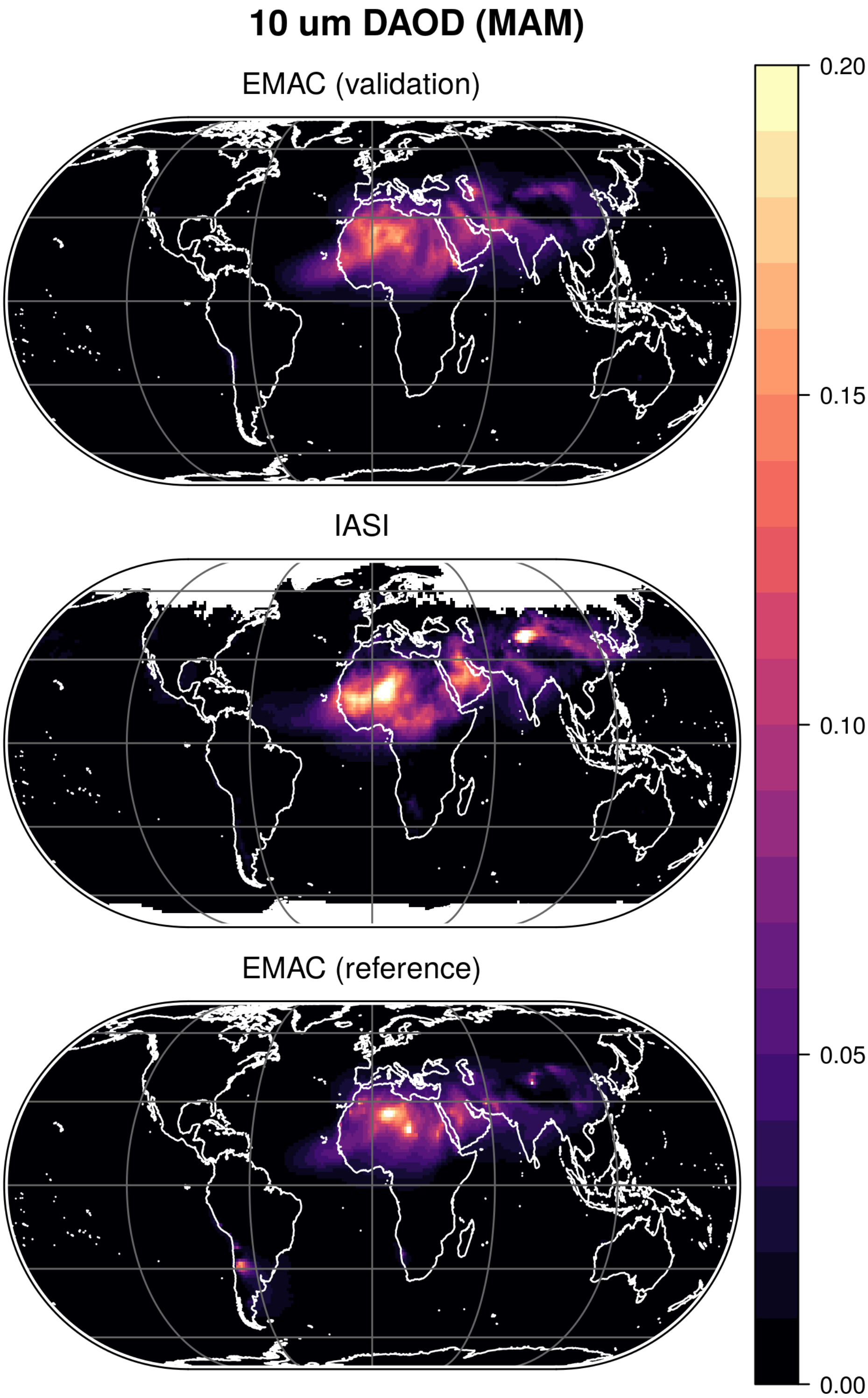

Figure S13: 10000 nm DAOD during spring (March, April, May) observed by IASI (centre) and simulated by EMAC with (“validation”, top) and without (“reference”, bottom) revision of the dust emission scheme.

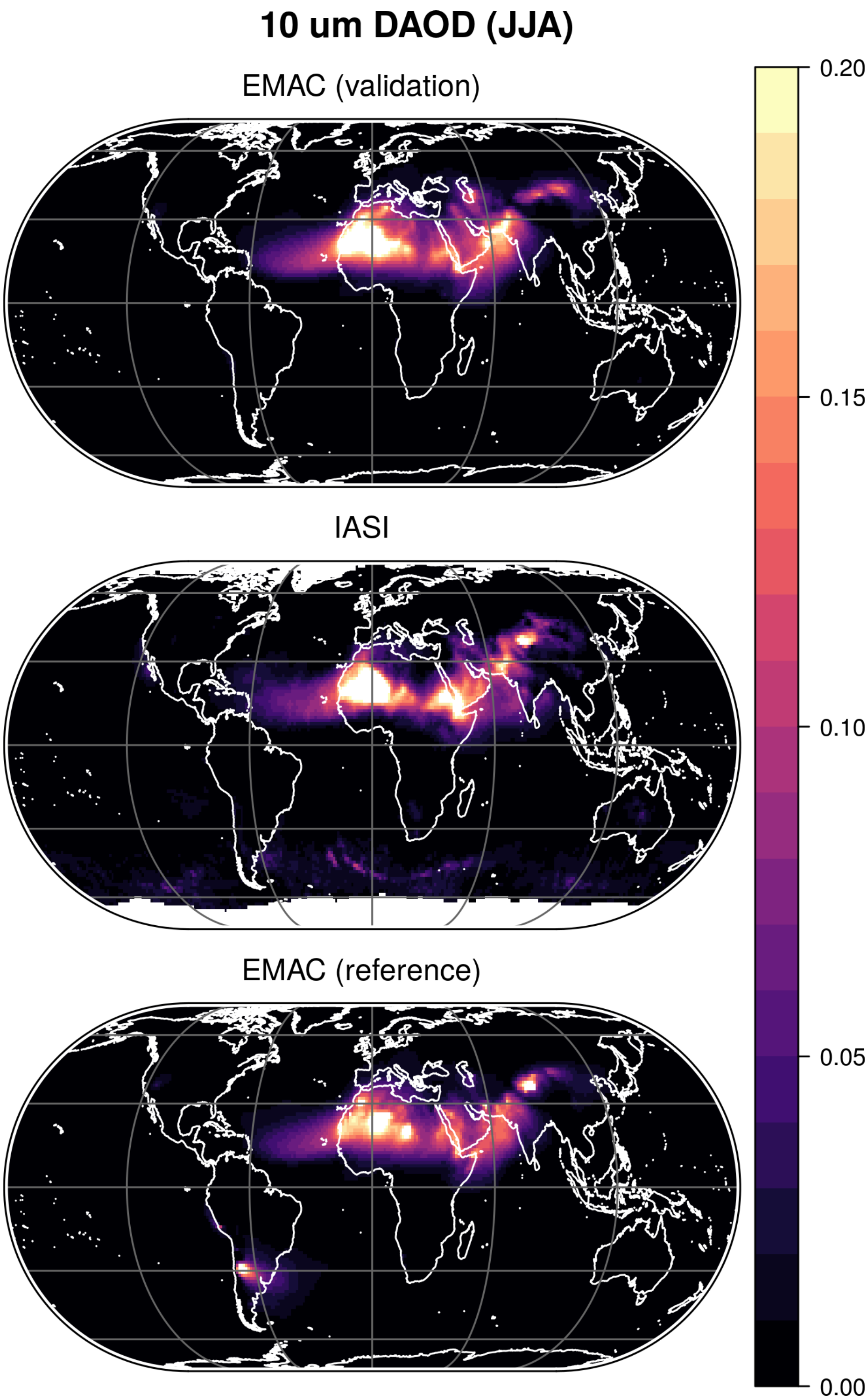

Figure S14: 10000 nm DAOD during summer (June, July, August) observed by IASI (centre) and simulated by EMAC with ("validation", top) and without ("reference", bottom) revision of the dust emission scheme.

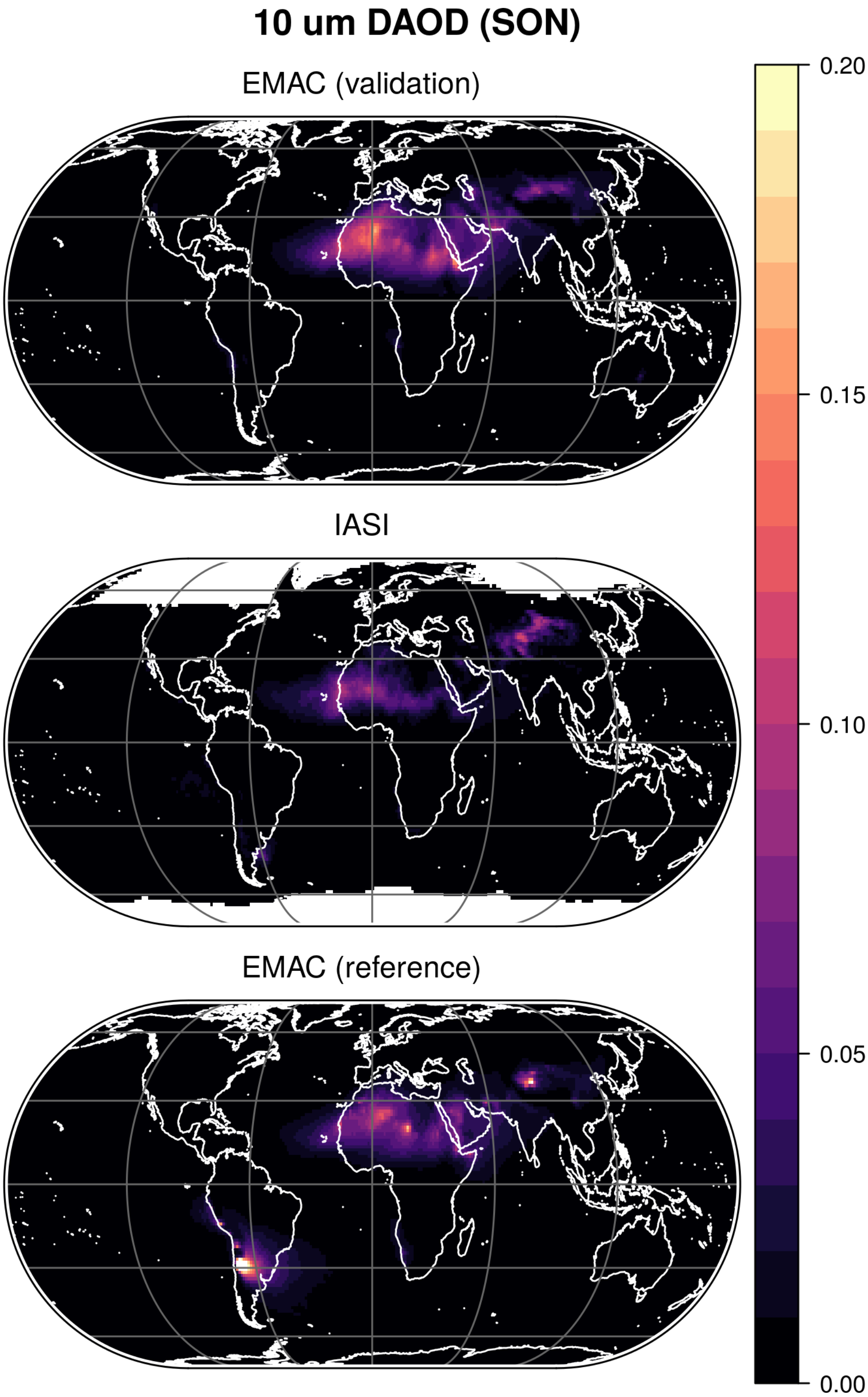

Figure S15: 10000 nm DAOD during autumn (September, October, November) observed by IASI (centre) and simulated by EMAC with ("validation", top) and without ("reference", bottom) revision of the dust emission scheme.

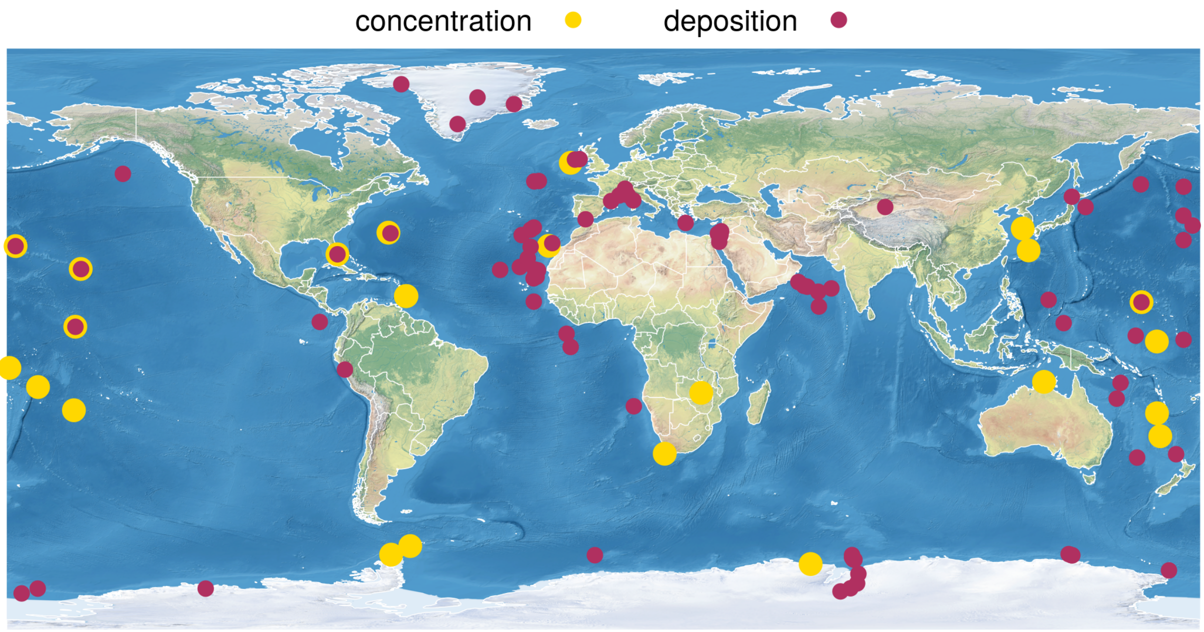

Figure S16: Sites with dust concentration and deposition observations available in the AERO-COM dust benchmark data (Huneeus et al. 2011).

Bibliography

Astitha, M., J. Lelieveld, M. Abdel Kader, A. Pozzer, and A. de Meij. 2012. "Parameterization of dust emissions in the global atmospheric chemistry-climate model EMAC: impact of nudging and soil properties." *Atmospheric Chemistry and Physics* 12 (22): 11057–83. doi:{10.5194/acp-12-11057-2012}.

Huneeus, N., M. Schulz, Y. Balkanski, J. Griesfeller, J. Prospero, S. Kinne, S. Bauer, et al. 2011. "Global Dust Model Intercomparison in Aerocom Phase I." *Atmospheric Chemistry and Physics* 11 (August): 7781–7816. doi:10.5194/acp-11-7781-2011.

Scholes, R.J., and E. Brown de Colstoun. 2011. "ISLSCP II Global Gridded Soil Characteristics." In *ISLSCP Initiative II Collection*, edited by Forrest G. Hall, G. Collatz, B. Meeson, S. Los, E. Brown de Colstoun, and D. Landis. ORNL Distributed Active Archive Center. doi:10.3334/ORNLDAAC/1004.

Shangguan, Wei, Yongjiu Dai, Qingyun Duan, Baoyuan Liu, and Hua Yuan. 2014. "A global soil data set for earth system modeling." *Journal of Advances in Modeling Earth Systems* 6 (1): 249–63. doi:10.1002/2013MS000293.